



# High fire-derived nitrogen deposition on central African forests

Marijn Bauters<sup>a,b,1</sup>, Travis W. Drake<sup>c</sup>, Hans Verbeeck<sup>b</sup>, Samuel Bodé<sup>a</sup>, Pedro Hervé-Fernández<sup>a,d</sup>, Phoebe Zito<sup>c,2</sup>, David C. Podgorski<sup>c,2</sup>, Faustin Boyemba<sup>e</sup>, Isaac Makelele<sup>e</sup>, Landry Cizungu Ntaboba<sup>f</sup>, Robert G. M. Spencer<sup>c</sup>, and Pascal Boeckx<sup>a</sup>

<sup>a</sup>Isotope Bioscience Laboratory–ISOFYS, Ghent University, 9000 Ghent, Belgium; <sup>b</sup>CAVElab, Computational and Applied Vegetation Ecology, Ghent University, 9000 Ghent, Belgium; <sup>c</sup>National High Magnetic Field Laboratory Geochemistry Group, Department of Earth, Ocean and Atmospheric Science, Florida State University, Tallahassee, FL 32306; <sup>d</sup>Laboratory of Hydrology and Water Management, Ghent University, 9000 Ghent, Belgium; <sup>e</sup>Plant Department, Faculty of Science, Université de Kisangani, Kisangani, Democratic Republic of Congo; and <sup>f</sup>Faculty of Agronomy, Université Catholique de Bukavu, BP 285 Bukavu, Democratic Republic of Congo

Edited by Peter M. Vitousek, Stanford University, Stanford, CA, and approved December 1, 2017 (received for review August 17, 2017)

**Atmospheric nitrogen (N) deposition is an important determinant of N availability for natural ecosystems worldwide. Increased anthropogenic N deposition shifts the stoichiometric equilibrium of ecosystems, with direct and indirect impacts on ecosystem functioning and biogeochemical cycles. Current simulation data suggest that remote tropical forests still receive low atmospheric N deposition due to a lack of proximate industry, low rates of fossil fuel combustion, and absence of intensive agriculture. We present field-based N deposition data for forests of the central Congo Basin, and use ultrahigh-resolution mass spectrometry to characterize the organic N fraction. Additionally, we use satellite data and modeling for atmospheric N source apportionment. Our results indicate that these forests receive 18.2 kg N hectare<sup>-1</sup> years<sup>-1</sup> as wet deposition, with dry deposition via canopy interception adding considerably to this flux. We also show that roughly half of the N deposition is organic, which is often ignored in N deposition measurements and simulations. The source of atmospheric N is predominantly derived from intensive seasonal burning of biomass on the continent. This high N deposition has important implications for the ecology of the Congo Basin and for global biogeochemical cycles more broadly.**

nitrogen deposition | central Africa | Congo Basin | biomass burning | FT-ICR-MS

**H**uman activities, such as the production of ammonium-based fertilizers and the burning of fossil fuels, have led to dramatic changes in the global N cycle over the past century (1). Increased levels of reactive N in the atmosphere have clear ramifications for ecosystems worldwide. Nitrogen is tightly coupled to carbon (C) in global biogeochemical cycles due to the metabolic need of plants and (micro)organisms. Furthermore, recent data analyses and modeling activities have shown that carbon dioxide (CO<sub>2</sub>) uptake by terrestrial ecosystems strongly depends on nutrient availability (2–4). This finding is important for tropical forests, which dominate the terrestrial C cycle and account for approximately one-third of global terrestrial gross primary productivity (5). This nutrient control on forests highlights the importance of quantifying atmospheric N deposition to understand and predict the global C cycle. This has prompted the Earth system modeling community to improve the implementation of nutrient cycles in their models, with varying consequences for the predicted effects of N deposition on C cycling in tropical forests (6–9). Indeed, model parameterization largely depends on the quantity and quality of empirical data used to constrain the simulations. Recently, global empirical N deposition data mapped from different monitoring networks showed a distinct lack of field-based estimates for the tropics (10). More importantly, the studies that do exist report typically solely the inorganic N inputs, overlooking the organic component in deposition. Recent reviews call attention to the importance of including this atmospheric organic N component, while pointing to

a complete lack of data from Africa (11, 12). They conclude that the effect of N deposition can only be understood if the organic component is consistently included and considered.

In short, there is no empirical organic N deposition data for African forests and, consequently, no insight into its potential sources. Some studies have suggested that a large proportion of organic N is sourced from the atmosphere and derived from biomass burning (13, 14). Satellite data coupled to biogeochemical models have identified the African continent as a key region for biomass burning, comprising 65% of the total global burnt area (i.e., 222 Mha yr<sup>-1</sup>) (15). Most of this biomass burning occurs as large seasonal wildfires in the savannas, with an estimated 78% of the tropical reactive N from savanna fire emissions sourced within the African savanna (4.3 of 5.5 Tg N yr<sup>-1</sup>) (16). Additionally, it was found that the net transfer of N from savannas to forests around the equator was larger in Africa than in South America and Asia due to the prevailing equatorward winds that carry emissions into the intertropical convergence zone. These models hint at the potential magnitude and composition of total N deposition on these remote forests, but have not been corroborated by field-based observational data to date. In this study, we directly measured N deposition on the ground in a remote forest in the central Congo Basin. Specifically, we collected biweekly water samples in the open field and under the forest canopy of two

## Significance

**Atmospheric N deposition affects productivity and biodiversity of forests worldwide. However, field-based estimates of atmospheric N deposition for tropical forests are extremely sparse. Our results from a monitoring network in the central Congo Basin exceed current regional N deposition simulations. Ultrahigh-resolution mass spectrometry and modeling techniques reveal that savannah biomass burning is the main source for this elevated atmospheric N deposition. Furthermore, a large fraction is deposited as organic N, which is typically not simulated or measured in monitoring networks. These high levels of N deposition have clear ramifications for the ecology and biogeochemistry of the Congo Basin.**

Author contributions: M.B., H.V., L.C.N., and P.B. designed research; M.B., T.W.D., F.B., I.M., R.G.M.S., and P.B. performed research; M.B., T.W.D., S.B., P.H.-F., P.Z., D.C.P., and R.G.M.S. contributed new reagents/analytic tools; M.B., T.W.D., S.B., D.C.P., and R.G.M.S. analyzed data; and M.B., T.W.D., H.V., and P.B. wrote the paper.

The authors declare no conflict of interest.

This article is a PNAS Direct Submission.

Published under the PNAS license.

<sup>1</sup>To whom correspondence should be addressed. Email: Marijn.Bauters@UGent.be.

<sup>2</sup>Present address: Pontchartrain Institute for Environmental Sciences, Department of Chemistry, University of New Orleans, New Orleans, LA 70148.

This article contains supporting information online at [www.pnas.org/lookup/suppl/doi:10.1073/pnas.1714597115/-DCSupplemental](http://www.pnas.org/lookup/suppl/doi:10.1073/pnas.1714597115/-DCSupplemental).

forest types. To unravel the origin of the N, we used both ultrahigh-resolution mass spectrometry and modeling techniques.

## Results and Discussion

Monitoring N deposition throughout a hydrological year in the remote forest of the central Congo Basin, we found a high total dissolved nitrogen (TDN) open-field (bulk) deposition of  $18.2 \text{ kg N ha}^{-1} \text{ yr}^{-1}$ , of which 70% was organic N. Throughfall, the precipitation collected under the forest's canopy, amounted to  $53.1 \pm 3.2 \text{ kg N ha}^{-1} \text{ yr}^{-1}$  in mixed forest, and  $37.5 \pm 4.2 \text{ kg N ha}^{-1} \text{ yr}^{-1}$  in monodominant forest, with roughly 50% organic N in both cases (mean  $\pm$  SD) (Table S1). The time series of deposition showed a consistent series of peaks at the onset of the rainy seasons in March and September, suggesting a strong contribution from previous dry deposition (Fig. 1). This elevated deposition was not expected at this remote site, because there is no industrial activity or intensive agriculture in the vicinity. Moreover, these measured N deposition rates already surpass the simulated deposition rates for 2030 (17).

To gain further insight into the source and composition of the organic fraction (50–70% of total N deposition) (Table S1), we characterized the compound classes of the organic components using ultrahigh-resolution Fourier transform ion cyclotron resonance mass spectrometry (FT-ICR-MS). The composition of dissolved organic matter (DOM) in the three sample types (i.e., open-field rainfall, mixed forest, and monodominant throughfall) showed a striking similarity (Fig. S1). For each sample type, the absolute and subgroup relative abundances of N-containing compounds were consistent (Fig. 2 A–C). The annual average molecular composition plotted in van Krevelen space also yielded, overall, very similar distributions (Fig. 2 D–F and Fig. S1). We found a high number of assigned molecular formulae in all sample types, with an average of 17,096, 16,955, and 15,627 for the open-field rainfall, mixed forest, and monodominant forest throughfall, respectively. Of these formulae, 52% contained at least one N atom on average, resulting in a large number of N-containing compounds with similar composition in all sample types (Fig. S1 and Table S1). One question that arises from these data is to what extent the increased organic N load in throughfall is caused by dry deposition versus canopy leaching. The relative abundances of compound classes in the three sample types, with a high percentage of unsaturated phenolics, closely resembles a previous study of glacier DOM on the Tibetan plateau, where atmospheric deposition was identified as the main source (18). The overall molecular similarity of the two forest types suggests that the throughfall enrichment of N is due to canopy interception of dry deposition rather than canopy leaching, as canopy leaching would be expected to result in a divergent compositional signature between the two forest types. In fact, we found only 2,811 and 2,459 unique formulae in the mixed and monodominant forest throughfall samples, respectively, that were not found in the open-field rainfall samples. Of these formulae, only 1,380 and 1,039 contained at least one N atom. These unique formulae only contributed 0.94% and 0.86% relative abundance to the total DOM signature for the mixed and monodominant forest samples, respectively (Fig. 2 D–F). Collectively, this qualitative compositional evidence suggests that the vast majority of N found in our forest throughfall samples was from atmospheric deposition.

Quantitatively measuring the contribution of canopy exchange and dry deposition in throughfall samples has proven to be a challenging task, especially in the tropics where appropriate methods still need to be developed (19). Rather than using  $\text{Na}^+$  or  $\text{Cl}^-$  as an inert tracer (Materials and Methods), we calculated an average condensed aromatic content using FT-ICR-MS data as proxy for fire-derived N deposition component of the organic fraction. Condensed aromatics are formed only through combustion and are therefore not a canopy leaching product (20).

The dissolved organic nitrogen (DON) deposition loads increased linearly with increasing average condensed aromatic content, which suggests that fire-derived dry deposition controls organic N loads in the throughfall (Fig. S2). The difference in N deposition and condensed aromatics content between mixed lowland and monodominant forests might be due to the increased heterogeneity of the mixed forest, which would lead to differing levels of aerosol interception of the canopies. *Gilbertiodendron dewevrei*, the monodominant species constituting a minimum of 60% of the basal area, is characterized by large leaves. Hypothetically, the combination of a homogenous canopy and large leaves might render them less efficient for dry deposition removal from the air, much like the described differences in fine dust removal efficiency between tree species (21). Altogether, these data suggest that organic N deposition found at all sites is predominantly sourced from biomass burning and not the forest canopy itself. We expect that at least part of the inorganic deposition comes from dry deposition as well, but there are no satisfactory techniques to further confirm this using the dataset.

Although the abundance of fires on the savanna borders has been shown before (16), our data suggest that the impact on central African forests in terms of N addition is much higher than expected. To investigate this link, we crossed existing datasets of daily fire pixels (recorded by MODIS satellites and processed through NASA's FIRMS system) with daily backward wind-trajectories as simulated for the study period by the Hybrid Single Particle Lagrangian Integrated Trajectories (HYSPPLIT) model of National Oceanic and Atmospheric Administration (NOAA) (Movie S1). This gave rise to an empirical fire load index (FLI) (Fig. 1A), which represents the number of fires that the winds directly above our sites passed over during the week before the sampling. A striking seasonality in this FLI showed that the local dry season is the peak season for fire arrivals for the central African rainforests. This was confirmed by extracting the black carbon column mass density (BCCMD) from NASA's Modern-Era Retrospective Analysis for Research and Applications version 2 (MERRA 2) model (Fig. 1A). Black carbon is a known combustion product, originating from either fossil fuel combustion or biomass burning (20), and hence can also serve as a proxy for the fire load of the atmosphere.

The intertropical convergence zone (ITCZ) shifts from the southern savanna border in January to the northern savanna border in July, inducing shifts in the rainy seasons for the savanna borders. As a result, the dry seasons oscillate inversely from the north to the south, in January to July, and back. During these shifts, the ITCZ passes over the central Congo Basin twice, inducing a bimodal rainfall pattern. It has been shown that the location of the ITCZ and the interoceanic confluence on the African continent causes biomass combustion products from the savanna borders to be transported in the direction of the equator during the dry season, and shifts of the ITCZ introduce seasonality in fire regime with latitude (Fig. 1) (22). These field-based observations, combined with molecular signatures of fire-derived organic compounds that correspond well with model-based fire inputs from the atmosphere, raise substantial questions as to the overall impact of high N deposition in central African forests. The fire abundance on the African continent has been chronically high during the last millennia (23, 24), suggesting that N deposition to the Congo Basin has also been high over this period. Additionally, given the agreement between the FLI and the BCCMD (Fig. 1), annual and monthly deposition maps and aerosol transport models suggest that the entire Congo Basin is subject to similar, if not higher, deposition loads (Fig. S3 and Movie S2). Currently available global simulation maps, which are used by modelers for reactive nitrogen loads, predict values for central Africa between 4 and 10 kg dissolved inorganic nitrogen (DIN)  $\text{ha}^{-1} \text{ yr}^{-1}$  (25–27). While these estimates correspond well with the DIN loads we

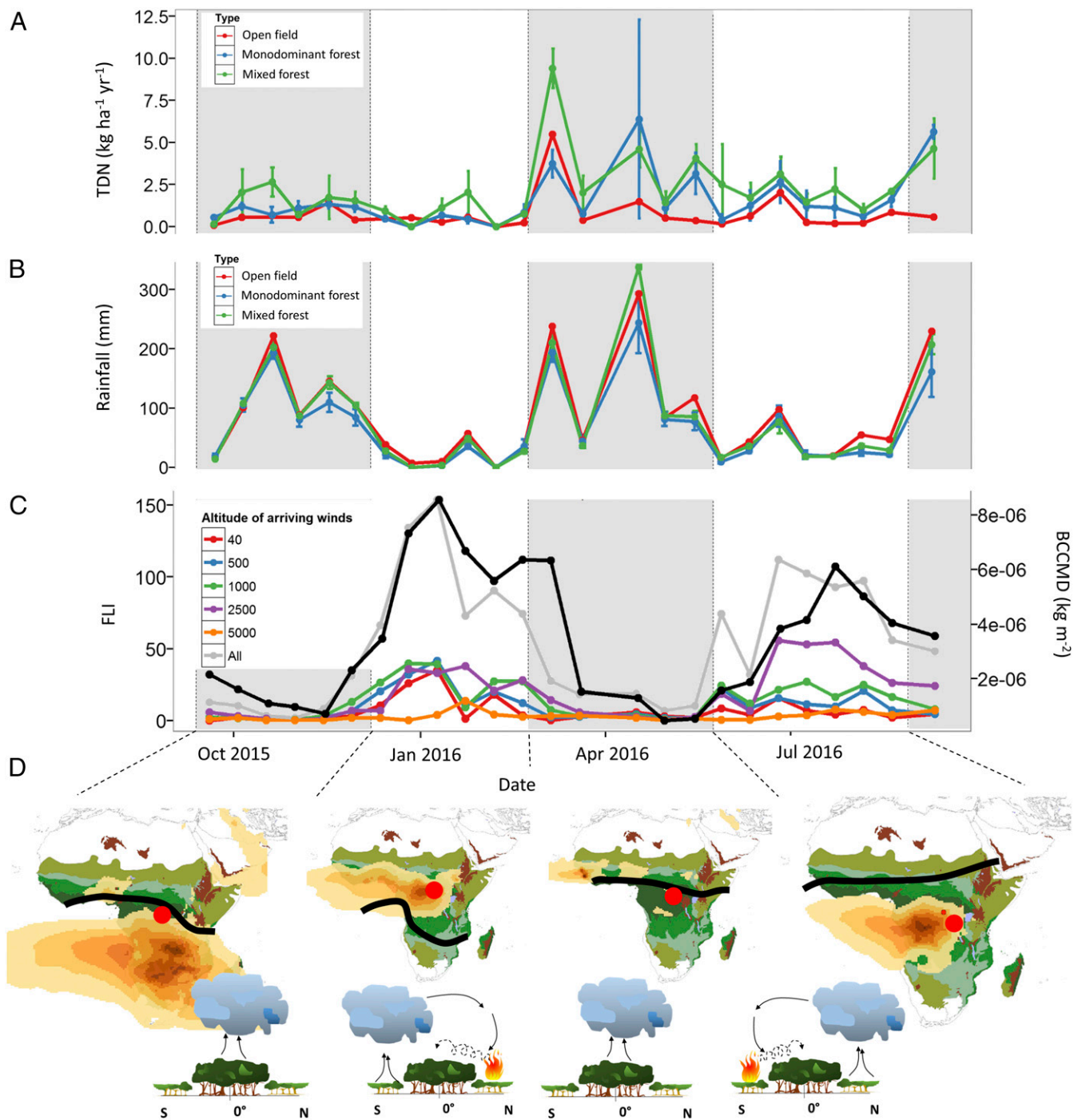


**Fig. 1.** Seasonality of TDN deposition, rainfall, and biomass burning-derived compound arrival. The graphs show (A) biweekly deposition of TDN in the open field (red), mixed lowland tropical forest (green), and monodominant lowland forest (blue), showing mean  $\pm$  SD values for each forest type, with additionally (B) the rainfall seasonality (millimeters) in the open field (red), mixed lowland tropical forest sites (green), and monodominant lowland forest sites (blue). (C) Evolution of our empirical FLI above our study site: that is, the number of fires that the winds directly above our sites passed over during the week before the sampling ( $\times 1,000$ ) at different altitudes (colors), along with the evolution of time-averaged BCCMD above the study site as simulated by MERRA-2 (black line). The gray and white zones denote the rainy and dry season, respectively. Lower maps (D) show the monthly averaged BCCMD for (from Left to Right) October 2015, and February, April, and July 2016, with increasing intensity from yellow to brown. Throughout the year, low pressure areas move from the northern savanna zone, over the equatorial forest, to the southern savannas and back, causing shifts in rainfall patterns around the ITCZ (approximate position indicated as a black line on the maps). Both natural fires, as well as those resulting from farmers preparing their land for the coming growing season, cause biomass burning products to arrive in the equatorial tropical forest during the dry season, with our study site indicated by the red dot on the maps. The coloration on the same map shows the ecosystem type delineation, with tropical rainforest in dark green.

found in the open field, they dramatically underestimate total N deposition because organic N is not accounted for, which was also shown by recent simulations (28). Although the bioavailability of

this organic N is still being studied (12, 29), the discrepancy between simulations and our data raises questions about the consequences of this high N deposition on forest functioning,

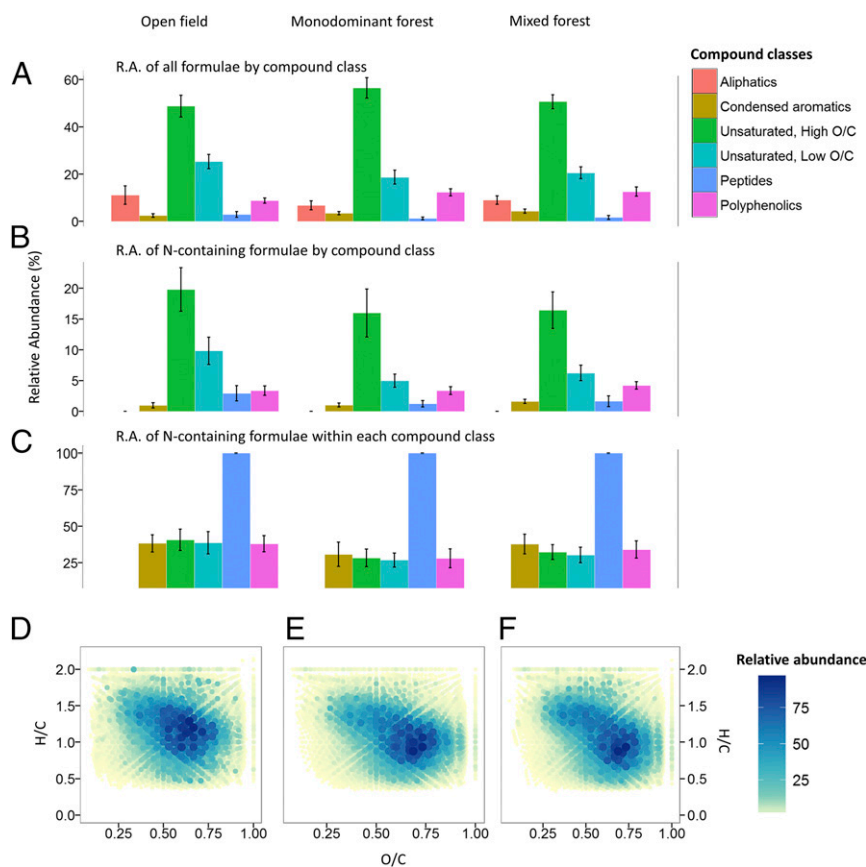


**Fig. 2.** Molecular characterization of rainfall and throughfall samples, based on a subset of samples from the open field and from one of the monodominant and one of the mixed forest plots, respectively. Relative abundance of different compound classes (A) of dissolved organic molecular formulae in the open-field rainfall and throughfall of monodominant and mixed lowland tropical forest samples, with (B) the relative abundance of nitrogen containing compounds in the samples, and (C) the relative abundance of nitrogen containing compounds within each separate compound class; molecular formulae (D–F) of the open rainfall, monodominant forest, and the mixed forest, respectively, plotted in the van Krevelen space. Relative abundance is the mean intensity of the plotted formula. Bars and error bars in A–C represent the mean over the samples per forest type  $\pm$ SD.

biodiversity, and the regional C budget of central African forests. The latter is of particular importance given that African forests currently represent one of the largest sources of uncertainty for the global CO<sub>2</sub> budget (30). It is generally assumed that productivity in lowland tropical forests is not N-limited (31, 32). Moreover, symbiotic N fixation by canopy trees is usually down-regulated in mature central African forests, confirming that N is cycled in excess (33). However, it remains unclear to what extent reactive N loads affect N and C cycling and biodiversity in tropical forests (34, 35). It is possible that the delivery of reactive N impacts forest structure, functioning, and biodiversity via effects on taxa, functional groups, and size classes (36, 37). We therefore suggest an urgent expansion of the monitoring efforts in the Congo Basin, to adjust and improve global and regional estimates of reactive nitrogen loads.

## Material and Methods

**Study Site.** The study was carried out in an old-growth tropical forest of Yoko, roughly 30-km south of Kisangani (N00°17'; E25°18'), in the Democratic Republic of the Congo. Vegetation at the study site is classified as semi-deciduous rainforest, and the climate falls within the Af-type (tropical rainforest climate), following the Köppen–Geiger classification. Soils in the region are typical deeply weathered and nutrient-poor Ferralsols, with very limited elevation differences and gentle slopes. The site has two dominant forest types: mixed lowland tropical forest and *Gilbertiodendron*-dominated forest, where >60% of the basal area consists of one species, *G. dewevrei*. Throughfall was sampled at three study plots of 40 × 40 m per forest type.

Additionally, we collected bulk precipitation in one location in the open field at a nearby deforested site.

**Data Collection.** Samples were collected from September 19, 2015 to September 10, 2016. Throughfall and bulk precipitation was collected using polyethylene funnels supported by a wooden pole of 1.5-m height, on which a polyethylene tube was attached to drain into a 5-L polyethylene container. A nylon mesh was placed in the neck of the funnel to avoid contamination by large particles. The container was buried in the soil and covered with black plastic to prevent the growth of algae and to keep the samples cool to minimize microbial activity. In each plot, we installed eight throughfall collectors in two rows of four, with ~8-m distance between all collectors. All plots were sampled every fortnight. On each sampling occasion, the water volume in each collector was measured in the field, and used recipients, funnels, and mesh were replaced by new ones, rinsed with distilled water. A volume-weighted composite sample was made per plot. The volume-weighted biweekly composite samples were filtered using a nylon membrane filter of 0.45  $\mu$ m before freezing, and then immediately stored in a freezer. Finally, the samples were sent in several batches to Ghent University (Belgium) for chemical analysis.

**Chemical Analysis and Empirical Data Analysis.** After transport to Belgium, NH<sub>4</sub><sup>+</sup> was determined colorimetrically by the salicylate–nitroprusside method (38) on an autoanalyzer (AA3; Bran and Luebbe). NO<sub>3</sub><sup>−</sup> was determined colorimetrically using the same auto-analyzer as NO<sub>2</sub> after reduction of NO<sub>3</sub><sup>−</sup> in a Cd–Cu column, followed by the reaction of the NO<sub>2</sub> with *N*-1-naphthylethylenediamine to produce a chromophore. DON can only be determined indirectly via measurement of TDN and subtraction of DIN, leading to additional analytical uncertainty. As discussed elaborately by Cornell et al. (40), there are three methods that are often used to determine

TDN in water samples: Kjeldahl digestion, persulfate oxidation, and high-temperature catalytic oxidation. At least for marine samples, no systematic biases have been found in method intercomparisons (39, 40). However, there is a risk of underestimating DON, because the main source of error of TDN determination is the incomplete conversion of DON to DIN (40). We used persulfate oxidation for the determination of TDN in the water sample. For this, a 1:1 oxidizing solution of NaOH, H<sub>3</sub>BO<sub>3</sub>, and K<sub>2</sub>S<sub>2</sub>O<sub>8</sub> is added to the sample, which is subsequently placed in an autoclave at 121 °C for 1 h to convert NH<sub>4</sub><sup>+</sup> and dissolved DON into NO<sub>3</sub><sup>-</sup> (41). In addition, a subset of samples was taken for bulk precipitation ( $n = 12$ ), for one of the mixed lowland plots ( $n = 23$ ), and for one of the monodominant plots ( $n = 19$ ) for further analysis by electrospray ionization (ESI) coupled with FT-ICR MS. Before extraction for FT-ICR MS, dissolved organic carbon (DOC) was analyzed. Therefore, samples were thawed under refrigeration (4 °C), acidified with 12N HCl to a pH of ~2, and measured via high-temperature catalytic oxidation on a TOC-analyzer (Shimadzu, Japan). DOC concentrations were determined as the mean of at least three replicate injections, for which the coefficient of variation was <2% (42). Samples were prepared for ESI-FT-ICR MS analysis by the solid-phase extraction (SPE) of DOM method (43). Briefly, filtered samples were acidified to pH 2.3 with HPLC-grade HCl before solid phase extraction on 100-mg Bond Elut PPL (Agilent Technologies) cartridges. Sample volume was adjusted depending on original DOC concentration to obtain 40 µg C per milliliter of methanol eluate. Negative ions produced by ESI from direct infusion of the methanol extracts at a concentration of 50 µg C mL<sup>-1</sup> were analyzed with a 21 T FT-ICR mass spectrometer (Florida State University, Tallahassee) (44). Each signal >6σ RMS baseline noise was assigned a molecular formula with EnviroOrg (45), and classified as condensed aromatic [modified aromaticity index ( $AI_{mod} \geq 0.67$ ), polyphenol ( $0.67 > AI_{mod} > 0.5$ ), unsaturated, low oxygen ( $AI_{mod} < 0.5$ ,  $H/C < 1.5$ ,  $O/C < 0.5$ ), unsaturated, high oxygen ( $AI_{mod} < 0.5$ ,  $H/C < 1.5$ ,  $O/C \geq 0.5$ ), aliphatic ( $H/C \geq 1.5$ ,  $n = 0$ ), and peptide ( $H/C \geq 1.5$ ,  $n > 0$ ) (18, 46), as defined in the Python script used in the analysis (47).

We used plot-averaged values for the bulk rainfall and throughfall volume data. The water flux for bulk rainfall and throughfall was calculated by dividing the average water volume by the surface area of the collector. Nitrogen deposition (TDN, DIN, and DON) was calculated by multiplying the water volume with the element concentration in that volume.

One of the most widely used methods to disentangle dry deposition from canopy leaching is the “canopy budget model,” which assumes that a natural tracer ion (most commonly Na<sup>+</sup>) is inert when deposited on the canopy. Additionally, the method is based on the calculation of an ion charge balance based cation deposition and computes canopy exchange interactions of NH<sub>4</sub><sup>+</sup>, NO<sub>3</sub><sup>-</sup> (48). However, several assumptions underlying this model seem to be challenged in tropical forest canopies, not least the apparent uptake

of Na<sup>+</sup> in some cases (49). Additionally, the model offers no theoretical basis for the calculation of organic N compounds from the canopy, other than the assumption that they are equally deposited on the canopy as the tracer ion. Given these factors, we chose not to apply this model here (19).

**Satellite and Wind Trajectory Analysis.** We calculated a FLI, representing the theoretical number of fires that were passed by the wind parcels that arrive above the experimental site. For this, we crossed a daily fire pixel dataset with backward wind trajectories ending at the site. The fire pixel dataset covering the entire African continent was obtained from NASA’s MODIS Collection 6 NRT (50). The backward wind trajectories were generated using the HYSPLIT model provided by the NOAA Air Resources Laboratory (51–54) with the GDAS half-degree archive meteorological dataset. For the entire study period, we generated one trajectory every 6 h, ending above the study site pixel for five different target altitudes (respectively: 40-, 500-, 1,000-, 2,500-, and 5,000-m above ground level), going back 1 wk. To cross the datasets, we counted fires within a 25-km zone around the modeled air parcels at each time point going back 24 h. The 24-h period was considered to take into account smoke from smoldering fires that might not have been detected by the VIIRS system at the time point in question. These fire counts were cumulated along the trajectory, resulting in a fire count per trajectory, and hence four fire counts per day. We then calculated the daily fire counts for every fortnight, resulting in the FLI for the concurrent sampling dates. Additionally, we extracted the hourly simulated BCCMD from above our study site from the MERRA-2 from the Goddard Earth Observing System Model, v5 (55). We subsequently calculated the average over this time series for all sample dates.

**ACKNOWLEDGMENTS.** We thank S. Vandevoorde for the help with the sample analysis. Some analyses and visualizations used in this paper were produced with the Giovanni online data system, developed and maintained by the NASA Goddard Earth Sciences Data and Information Services Center. We also acknowledge the use of data and imagery from LANCE FIRMS operated by the NASA/Goddard Space Flight Center/Earth Science Data and Information System with funding provided by NASA/HQ. This research has been supported by the Belgian Development Cooperation through VLIR-UOS, both through a personal scholarship (to M.B.) and project funding. VLIR-UOS supports partnerships between universities and university colleges in Flanders (Belgium) and the South looking for innovative responses to global and local challenges. Visit [www.vliruos.be](http://www.vliruos.be) for more information. Acquisition of mass spectra was supported by the National Science Foundation Division of Materials Research (DMR-11-57490). T.W.D., D.C.P., and R.G.M.S. were supported by the Winchester Foundation and partially by National Science Foundation Grant OCE-1464396. P.H.-F. is funded by Programa de Formación de Personal Avanzado Consejo Nacional de Investigaciones Científicas y Tecnológicas, BECAS Chile.

- Galloway JN, et al. (2008) Transformation of the nitrogen cycle: Recent trends, questions, and potential solutions. *Science* 320:889–892.
- Fernandez-Martinez M, et al. (2014) Nutrient availability as the key regulator of global forest carbon balance. *Nat Clim Chang* 4:471–476.
- Peñuelas J, Sardans J, Rivas-ubach A, Janssens IA (2012) The human-induced imbalance between C, N and P in Earth’s life system. *Glob Chang Biol* 18:3–6.
- Wieder WR, Cleveland CC, Smith WK, Todd-Brown K (2015) Future productivity and carbon storage limited by terrestrial nutrient availability. *Nat Geosci* 8:441–444.
- Beer C, et al. (2010) Terrestrial gross carbon dioxide uptake: Global distribution and covariation with climate. *Science* 329:834–839.
- Sokolov AP, et al. (2008) Consequences of considering carbon-nitrogen interactions on the feedbacks between climate and the terrestrial carbon cycle. *J Clim* 21: 3776–3796.
- Thornton PE, et al. (2009) Carbon-nitrogen interactions regulate climate-carbon cycle feedbacks: Results from an atmosphere-ocean general circulation model. *Biogeosciences* 6:2099–2120.
- Zaehle S, Friend AD (2010) Carbon and nitrogen cycle dynamics in the O-CN land surface model: 1. Model description, site-scale evaluation, and sensitivity to parameter estimates. *Global Biogeochem Cycles* 24:1–13.
- Thomas RQ, Brookshire ENJ, Gerber S (2015) Nitrogen limitation on land: How can it occur in Earth system models? *Glob Chang Biol* 21:1777–1793.
- Jia Y, et al. (2016) Global inorganic nitrogen dry deposition inferred from ground- and space-based measurements. *Sci Rep* 6:19810.
- Cape JN, Cornell SE, Jickells TD, Nemitz E (2011) Organic nitrogen in the atmosphere—Where does it come from? A review of sources and methods. *Atmos Res* 102:30–48.
- Cornell SE (2011) Atmospheric nitrogen deposition: Revisiting the question of the importance of the organic component. *Environ Pollut* 159:2214–2222.
- Mace KA, Artaxo P, Duce RA (2003) Water-soluble organic nitrogen in Amazon Basin aerosols during the dry (biomass burning) and wet seasons. *J Geophys Res* 108:4512.
- Ito A, Lin G, Penner JE (2015) Global modeling study of soluble organic nitrogen from open biomass burning. *Atmos Environ* 121:103–112.
- van der Werf GR, et al. (2006) Interannual variability in global biomass burning emissions from 1997 to 2004. *Atmos Chem Phys* 6:3423–3441.
- Chen Y, et al. (2010) Nitrogen deposition in tropical forests from savanna and deforestation fires. *Glob Chang Biol* 16:2024–2038.
- Reay DS, Dentener F, Smith P, Grace J, Feely RA (2008) Global nitrogen deposition and carbon sinks. *Nat Geosci* 1:430–437.
- Spencer RGM, et al. (2014) Source and biolability of ancient dissolved organic matter in glacier and lake ecosystems on the Tibetan Plateau. *Geochim Cosmochim Acta* 142: 64–74.
- Hofhansl F, et al. (2011) Topography strongly affects atmospheric deposition and canopy exchange processes in different types of wet lowland rainforest, Southwest Costa Rica. *Biogeochemistry* 106:371–396.
- Golberg E (1985) Black carbon in the environment. *J Am Vet Med Assoc* 244:353–354.
- Chen L, Liu C, Zhang L, Zou R, Zhang Z (2017) Variation in tree species ability to capture and retain airborne fine particulate matter (PM<sub>2.5</sub>). *Sci Rep* 7:3206.
- Cachier H, Ducret J (1991) Influence of biomass burning on equatorial African rains. *Nature* 352:228–230.
- Archibald S, Staver AC, Levin SA (2012) Evolution of human-driven fire regimes in Africa. *Proc Natl Acad Sci USA* 109:847–852.
- Marlon JR, et al. (2009) Climate and human influences on global biomass burning over the past two millennia. *Nat Geosci* 2:307.
- Dentener F, et al. (2006) Nitrogen and sulfur deposition on regional and global scales: A multimodel evaluation. *Global Biogeochem Cycles* 20:GB4003.
- Wang R, et al. (2017) Global forest carbon uptake due to nitrogen and phosphorus deposition from 1850 to 2100. *Glob Chang Biol* 23:4854–4872.
- Vet R, et al. (2014) A global assessment of precipitation chemistry and deposition of sulfur, nitrogen, sea salt, base cations, organic acids, acidity and pH, and phosphorus. *Atmos Environ* 93:3–100.
- Kanakidou M, et al. (2016) Past, present, and future atmospheric nitrogen deposition. *J Atmos Sci* 73:2039–2047.
- Bronk DA, See JH, Bradley P, Killberg L (2007) DON as a source of bioavailable nitrogen for phytoplankton. *Biogeosciences* 4:283–296.

30. Ciais P, et al. (2011) The carbon balance of Africa: Synthesis of recent research studies. *Philos Trans R Soc A* 369:2038–2057.
31. Vitousek PM, Sanford RL (1986) Nutrient cycling in moist tropical forest. *Annu Rev Ecol Syst* 17:137–167.
32. Hedin LO, Brookshire ENNJ, Menge DNLL, Barron AR (2009) The nitrogen paradox in tropical forest ecosystems. *Annu Rev Ecol Syst* 40:613–635.
33. Bauters M, Mapenzi N, Kearsley E, Vanlauwe B, Boeckx P (2016) Facultative nitrogen fixation by legumes in the central Congo Basin is downregulated during late successional stages. *Biotropica* 48:281–284.
34. Hietz P, et al. (2011) Long-term change in the nitrogen cycle of tropical forests. *Science* 334:664–666.
35. Janssens IA, et al. (2010) Reduction of forest soil respiration in response to nitrogen deposition. *Nat Geosci* 3:315–322.
36. Alvarez-Clare S, Mack MC, Brooks M (2013) A direct test of nitrogen and phosphorus limitation to net primary productivity in a lowland tropical wet forest. *Ecology* 94:1540–1551.
37. Bobbink R, et al. (2010) Global assessment of nitrogen deposition effects on terrestrial plant diversity: A synthesis. *Ecol Appl* 20:30–59.
38. Mulvaney RL (1996) Nitrogen–Inorganic forms. *SSSA Book Series: Methods of Soil Analysis. Part 3—Chemical Methods*, 5.3:1123–1184.
39. Sharp JH, et al. (2002) A preliminary methods comparison for measurement of dissolved organic nitrogen in seawater. *Mar Chem* 78:171–184.
40. Cornell SE, Jickells TD, Cape JN, Rowland AP, Duce RA (2003) Organic nitrogen deposition on land and coastal environments: A review of methods and data. *Atmos Environ* 37:2173–2191.
41. Lachouani P, Frank AH, Wanek W (2010) A suite of sensitive chemical methods to determine the  $\delta^{15}\text{N}$  of ammonium, nitrate and total dissolved N in soil extracts. *Rapid Commun Mass Spectrom* 24:3615–3623.
42. Mann PJ, et al. (2012) Controls on the composition and lability of dissolved organic matter in Siberia's Kolyma River basin. *J Geophys Res* 117:1–15.
43. Dittmar T, Koch B, Hertkorn N, Kattner G (2008) A simple and efficient method for the solid-phase extraction of dissolved organic matter (SPE-DOM) from seawater. *Limnol Oceanogr Methods* 6:230–235.
44. Hendrickson CL, et al. (2015) 21 Tesla Fourier transform ion cyclotron resonance mass spectrometer: A national resource for ultrahigh resolution mass analysis. 26:1626–1632.
45. Corilo Y (2015) EnviroOrg (Florida State University, Tallahassee, FL).
46. Koch BP, Dittmar T (2006) From mass to structure: An aromaticity index for high-resolution mass data of natural organic matter. *Rapid Commun Mass Spectrom* 20:926–932, and erratum (2015) 34:250.
47. Hemingway JD (2017) Fouriertransform: Open-Source Tools for FT-ICR MS Data Analysis. Available at <https://github.com/FluvialSeds/fouriertransform>. Accessed January 2017.
48. Staelens J, Houle D, De Schrijver A (2008) Calculating dry deposition and canopy exchange with the canopy budget model: Review of assumptions and application to two deciduous forests. *Water Air Soil Pollut* 191:149–169.
49. Tobón C, Sevink J, Verstraten JM (2004) Solute fluxes in throughfall and stemflow in four forest ecosystems in northwest Amazonia. *Biogeochemistry* 70:1–25.
50. NASA, MODIS Collection 6 NRT hotspot/Active fire detections MCD14DL. Available at <https://earthdata.nasa.gov/earth-observation-data/near-real-time/firms>. Accessed January 2017.
51. Draxler RR, Hess GD (1998) An overview of the HYSPLIT\_4 modelling system for trajectories, dispersion, and deposition. *Aust Meteorol Mag* 47:295–308.
52. Stein AF, et al. (2015) NOAA's HYSPLIT atmospheric transport and dispersion modeling system. *Bull Am Meteorol Soc* 96:2059–2077.
53. Draxler RR, Hess GD (1997) Description of HYSPLIT\_4 Modeling System (NOAA Air Resources Laboratory, Silver Spring, MD), Technical Report ERL ARL-224.
54. Draxler RR (1999) *HYSPLIT\_4 User's Guide* (NOAA Air Resource Laboratory, Silver Spring, MD), Technical Report ERL ARL-224.
55. Global Modeling and Assimilation Office, MERRA-2 tavg1\_2d\_aer\_Nx: 2d,1-Hourly, Time-averaged,Single-Level,Assimilation,Aerosol Diagnostics V5.12.4. Available at [https://disc.sci.gsfc.nasa.gov/datasets/M2T1NXAER\\_V5.12.4/summary?keywords=merra](https://disc.sci.gsfc.nasa.gov/datasets/M2T1NXAER_V5.12.4/summary?keywords=merra). Accessed December 2016.